Cross-section measurements of the ^{156}Dy$(n, 2n)$ ^{155}Dy reaction at neutron energies higher than 17 MeV

E. Georgali [1] N. Patronis,[1] A. Anastasiadis [2,3] X. Aslanoglou,[1] M. Axiotis [4] S. Chasapoglou [5] Z. Eleme,[1]
S. Harissopulos [4] A. Kalamara [5,6] M. Kokkoris [5] A. Lagoyannis [4] E. Mitsi [5] M. I. Savva [6]
I. E. Stamatelatos [6] T. Vasilopoulou [6] and R. Vlastou [5]

[1]*Department of Physics, University of Ioannina, 45110 Ioannina, Greece*
[2]*Department of Physics and Astronomy, Uppsala University, SE-751 05 Uppsala, Sweden*
[3]*Swedish Radiation Safety Authority, SE-171 16 Stockholm, Sweden*
[4]*Tandem Accelerator Laboratory, Institute of Nuclear and Particle Physics, N.C.S.R. "Demokritos", Aghia Paraskevi, 15310 Athens, Greece*
[5]*Department of Physics, National Technical University of Athens, Zografou Campus, 15780 Athens, Greece*
[6]*Institute of Nuclear and Radiological Sciences, Technology, Energy and Safety, N.C.S.R. "Demokritos",
Aghia Paraskevi, 15310 Athens, Greece*

In the present work the cross section of the ^{156}Dy $(n, 2n)$ ^{155}Dy reaction ($E_{th} = 9.51$ MeV) was measured at neutron beam energies above 17 MeV: 17.1, 18.1, and 19.0 MeV. The irradiations were performed at the 5.5-MV tandem accelerator of the Institute of Nuclear and Particle Physics at N.C.S.R. "Demokritos", where quasi-monoenergetic neutron beams were produced via the ^{3}H (d, n) ^{4}He reaction. The cross-section measurements were performed by means of the activation technique relative to the ^{27}Al (n, α) ^{24}Na reference reaction. Within the present work the experimental study is framed by theoretical calculations performed via the TALYS code (version 1.95).

I. INTRODUCTION

The accurate knowledge of the cross section of nuclear reactions is of prime importance for fundamental research, dosimetry, and the applications of nuclear technology [1]. In particular, the study of (n, xn) reactions is significant for the development of nuclear energy technology, as these reactions on structural materials of the reactors may affect the neutron flux as well as the neutron economy in these systems.

In the framework of fundamental research and as mentioned in the work of Goriely *et al.* [2], multiparticle emission may play a role in nuclear astrophysics. More specifically, according to Ref. [2], the $(n, 2n)$ channel may dominate the (n, γ) channel at relatively high temperatures. This could play a crucial role in the nucleosynthesis of neutron-rich isotopes and, hence, in the r-process nucleosynthesis. Therefore, the assumption that the multiparticle emission is negligible at astrophysics-relevant energies needs to be tested. For this reason, the cross-section measurements of the $(n, 2n)$ reaction channel are important.

Accordingly, a systematic study of neutron-induced nuclear reactions for a particular mass region utilizing in parallel the technological and simulation advances [3] constitutes a valuable tool both for nuclear technology and fundamental research. The present work is part of a systematic study that started from our group some years ago [4,5] and concerns the measurement of the $(n, 2n)$ reaction channel for the medium- to heavy-mass region. Through the present work the ^{156}Dy $(n, 2n)$ ^{155}Dy reaction has been measured at energies above 17 MeV. According to our knowledge, the experimental

data for this reaction in the literature are limited in a narrow energy range between 13.5 and 15 MeV [6–11].

^{156}Dy is the lightest isotope of the seven stable isotopes of the Dy element, which are presented in Table I along with their natural abundances [12]. This property constitutes an extra motivation for the performance of the present work, as this work is a continuation of our previous study for the $(n, 2n)$ reaction on stable but neutron-deficient isotopes [5].

In the next sections the experimental conditions and the data analysis are presented. In addition, the theoretical calculations as performed via the broadly used statistical code TALYS (version 1.95) [13] are discussed.

II. EXPERIMENTAL PROCEDURE

A. Irradiations setup

The cross section of the ^{156}Dy $(n, 2n)$ ^{155}Dy reaction was measured via the activation technique relative to the ^{27}Al (n, α) ^{24}Na reference reaction [14]. Three irradiations were performed at 17.1-, 18.1-, and 19.0-MeV neutron beam energies. The duration of each irradiation was between 18 and 21 h. The neutron beams were produced through the ^{3}H (d, n) ^{4}He reaction ($Q = 17.6$ MeV) at the 5.5-MV Tandem accelerator of N.C.S.R. "Demokritos".

In the irradiations three foils of natural Dy (one for each irradiation) were used. The Dy foils had a diameter of 13 mm and their thicknesses were 0.9, 0.9, and 0.8 cm, respectively. During the irradiations, each of them was placed between Al monitor foils of equal diameter.

TABLE I. The stable isotopes of the Dy element and the corresponding abundances [12].

Dy isotopes	natural abundance (%)
^{156}Dy	0.056 ± 0.003
^{158}Dy	0.095 ± 0.003
^{160}Dy	2.329 ± 0.018
^{161}Dy	18.889 ± 0.042
^{162}Dy	25.475 ± 0.036
^{163}Dy	24.896 ± 0.042
^{164}Dy	28.260 ± 0.054

Deuteron beams of 300-nA intensity were impinging on a 2.1 mg/cm^2 Ti-tritiated target. The Ti-tritiated target was supported by a 1-mm-thick Cu foil for optimum heat conduction purposes. Two 5-μm-thick Mo foils were placed in front of the Ti-tritiated target serving as energy degraders of the deuteron beam. During the irradiations the target flange was air-cooled. The foils were irradiated at 0° with respect to the deuteron beam at a distance of 2.3 and 2.4 cm from the Ti-tritiated target.

The energy distribution of the neutron beam was determined via the NEUSDESC code [15], developed at JRC-Geel. NEUSDESC makes also use of the SRIM-2008 Monte Carlo simulation program [16]. SRIM-2008 calculates the energy loss in the Mo foils and the Ti-tritiated target by taking into account the stochastic nature of the phenomenon. In Fig. 1 the energy distribution of the neutron beams is presented as calculated by NEUSDESC. The energy distributions are normalized to the total neutron beam flux (n/cm^2) which resulted from the reference foils. In addition to NEUSDESC, simulations of the

energy distribution of neutron beams were performed via the GEANT4 Monte Carlo simulation toolkit [17], by taking into account the deuteron beam transportation through the beam line optics elements and by considering the full configuration of the Ti-tritiated target. The results of the two codes are in agreement with each other.

During the irradiations the deuteron beam current on the Ti-tritiated target was recorded and was used for the accurate calculation of the f_B correction factor, which is presented in Sec. III. In this way, any fluctuations of the neutron beam were taken into account in the measurement of the cross sections.

B. Activity measurements

The irradiations were followed by the measurements of the induced activity of the irradiated Dy samples and reference foils.

The activity of the Dy samples following the ^{155}Dy decay [18] was measured by means of an 80% relative efficiency high-purity germanium (HPGe) detector at a distance of only 1 cm with respect to the detector window so as to compensate for the very low abundance of ^{156}Dy (0.056%) in the natural samples used.

Such a close detection geometry causes limitations in the activity measurements not only of the main sample but also of the efficiency calibration sources, due to the coincidence summing effect which becomes significant as the sample to detector window distance is reduced. For this reason, the detector efficiency at the detection geometry used for the energies of the transitions following the ^{155}Dy decay was determined using the GEANT4 simulation code. More specifically, the detector was characterized through GEANT4 so that
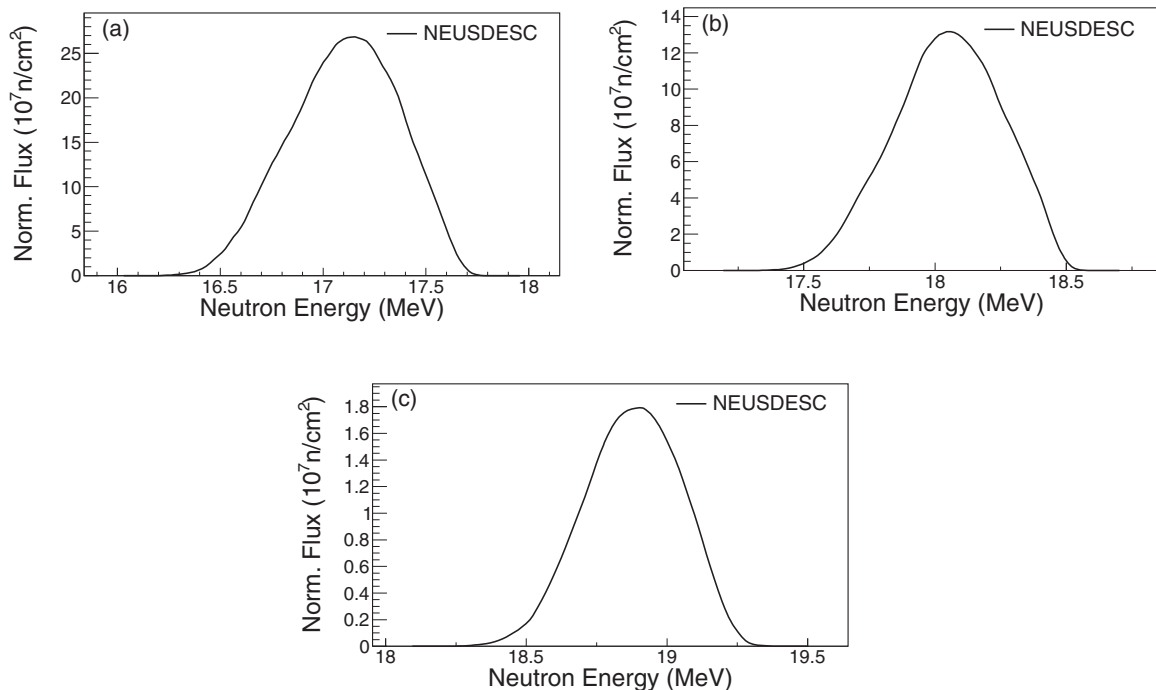

FIG. 1. The neutron beam energy distribution as resulting from the NEUSDESC code [15] for each neutron beam energy: (a) 17.1 ± 0.3 MeV, (b) 18.1 ± 0.2 MeV, and (c) 19.0 ± 0.2 MeV. The distributions are normalized to the total neutron beam flux.
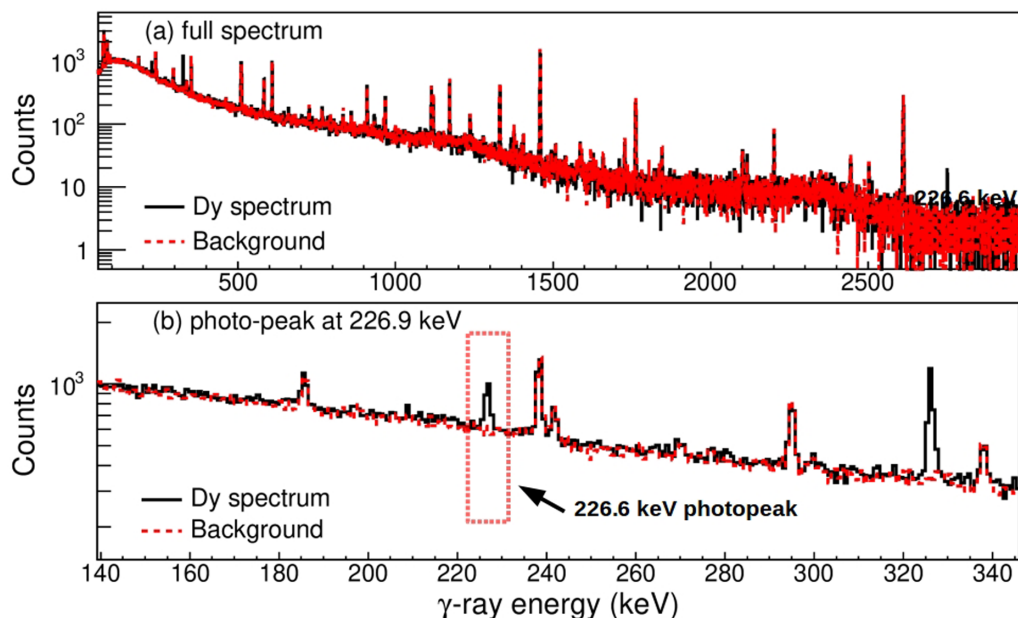
FIG. 2. The spectrum of ^{155}Dy recorded after the irradiation with the neutron beam at 17.1 MeV, along with the corresponding background spectrum of equal measurement time (16.8 h). Panel (a) corresponds to the full spectrum, whereas the panel (b) corresponds to the energy region around the main γ ray emitted by ^{155}Dy (226.9 keV).

the experimental efficiency and counting rate data of an ^{152}Eu [19] point source were reproduced via the simulations for various source to detector distances. The counting-rate term refers to close source to detector distances, where the counting integral of full-energy peaks is affected by the coincidence-summing effect. In the simulations the counting rates of the decay energies of ^{152}Eu were reproduced considering the decay scheme of ^{152}Eu. Details on the GEANT4 modeling of the detector and the performance of the simulations with respect the reproduction of experimental calibration data can be seen in Ref. [4].

Figure 2 illustrates the recorded spectrum from the ^{155}Dy decay after the irradiation of the Dy sample with the 17.1-MeV neutron beam, along with the background spectrum of equal data acquisition time (16.8 h). As shown in Fig. 2, the photopeaks contained in both spectra match each other except for the two photopeaks at 226.9 and 326.3 keV. The 226.9-keV γ ray is emitted by ^{155}Dy, whereas the 326.3-keV γ ray is emitted by ^{157}Dy, which is the product nucleus of the ^{158}Dy $(n, 2n)$ ^{157}Dy and ^{156}Dy(n, γ) ^{157}Dy interfering reactions. A zoom of the energy region around the 226.9-keV peak is plotted in Fig. 2(b).

As mentioned above, the efficiency of the detector at 226.9 keV was determined via the GEANT4 model of the detector. Corrections due to the self-attenuation of the emitted γ rays were taken into account in the efficiency calibration

by including the Dy samples' geometry and material in the GEANT4 simulations, whereas corrections due to coincidence summing were considered by including the full-decay scheme of ^{155}Dy in the simulations as well.

The induced activity of the reference foils was measured by a 40% relative efficiency HPGe detector at 7.3- and 11.1-cm distances with respect to the detector window. The efficiency of the detector at the decay energy of ^{24}Na [20] at 1368.6 keV was also determined through the GEANT4 characterization of the detector. As in the case of the previously mentioned HPGe detector, the simulation of the geometry of the detector was performed so that the experimental efficiency and counting-rate data of an ^{152}Eu point source were reproduced for different source to detector distances. After the detector characterization the efficiency at 1368.6 keV was calculated including in the simulations the foil dimensions and material, as well as the full-decay scheme of ^{24}Na. In this way, self-attenuation and coincidence-summing effect corrections were incorporated into the efficiency calculations.

In Table II the decay data of ^{155}Dy and ^{24}Na are summarized.

III. DATA ANALYSIS

In the present study the cross section of the ^{156}Dy $(n, 2n)$ ^{155}Dy reaction was determined via the activation

TABLE II. Decay properties of the product nuclei.

Product nucleus	Half-life	γ-ray energy (keV)	Intensity per decay (%)
^{155}Dy [18]	(9.9 ± 0.2) h	226.9	68.7 ± 1.6
^{24}Na [20]	(14.997 ± 0.012) h	1368.6	99.9936 ± 0.0015

TABLE III. Summary of the irradiation and measurement parameters of the Dy samples.

	17.1 MeV	18.1 MeV	19.0 MeV
Irradiation time (h)	19.5	18.6	20.6
Time-integrated flux ($\times 10^9$ n/cm^2)	9.96 ± 0.69	4.77 ± 0.33	5.72 ± 0.40
Decay correction factor f_B	0.5320	0.5752	0.5295
Measurement time (h)	16.8	14.3	16.3

technique. The induced activity A which was measured via the 226.9-keV γ ray is given by

$$A = \frac{I\varepsilon N_0 e^{-\lambda t_w}(1 - e^{-\lambda t_m})}{C_{\mathrm{DT}}}, \qquad (1)$$

where I is the intensity of the γ ray and ε is the efficiency of the detector at this γ-ray energy for the geometry of measurement. The term N_0 is the number of activated nuclei at the end of the irradiation, whereas the terms t_m and t_w stand for the activity measurement time and the time interval between the end of the irradiation and the start of the measurement ("waiting time"), respectively. The term λ is the decay constant of the product nucleus. The factor C_{DT} is the correction factor for the dead time of the data acquisition system. It was calculated as the ratio of the "real time" to the "live time" of the data acquisition system, and in any case it was found negligible.

The self-attenuation and the coincidence-summing effect corrections, as described in the previous section, were taken into account in the determination of the efficiency of the detector for the 226.9-keV γ ray through the GEANT4 simulations.

The cross section σ is given by

$$\sigma = \frac{N_0}{\Phi N_T f_B}, \qquad (2)$$

where Φ is the time-integrated neutron beam flux and N_T is the number of nuclei in the sample. The f_B term is the correction factor for the activated nuclei decay during the irradiation (t_{ir}) and it is calculated including the neutron beam fluctuations as follows:

$$f_B = \frac{\int_0^{t_{\mathrm{ir}}} \mathrm{flux}(t) e^{\lambda t} dt}{\int_0^{t_{\mathrm{ir}}} \mathrm{flux}(t) dt} e^{-\lambda t_{\mathrm{ir}}}. \qquad (3)$$

By combining Eqs. (1) and (2), the formula of the cross section is obtained:

$$\sigma = \frac{AC_{\mathrm{DT}}}{\Phi N_T \varepsilon I e^{-\lambda t_w}(1 - e^{-\lambda t_m})f_B}. \qquad (4)$$

The neutron beam flux was determined via the reference reaction. The corresponding cross sections at the neutron beam energies were obtained from the IRDFF-1.05 library [14].

In Table III the irradiation time and the activity measurement time for the Dy samples are presented along with the time-integrated neutron beam flux and the f_B correction factor for each irradiation.

In Table IV a compilation of the individual uncertainties is summarized. The cross-section uncertainty was determined by summing up quadratically all the possible individual uncertainties. The dominant source of uncertainty was the statistical uncertainty of the photopeak at 226.9 keV. An important contribution comes also from the neutron flux and the ^{156}Dy abundance uncertainties. The intensity of the 226.9-keV γ ray and the detector efficiency uncertainties have a less important effect.

IV. TALYS CALCULATIONS

The cross-section measurements of the present study, as well as the previous ones [21], were compared with calculations performed using the broadly used statistical code TALYS (version 1.95).

The $(n, 2n)$ reaction channel on the heavy- to medium-mass region, which ^{156}Dy belongs to, is dominated by the compound-nucleus mechanism for the energies considered in the present work. In TALYS the compound-nucleus calculations

TABLE IV. Compilation of uncertainties (in %).

| E_n (MeV)	17.1	18.1	19.0
Reference reaction		^{24}Al (n, α) ^{24}Na	
Reference reaction cross section	0.83	0.98	1.19
Neutron flux	7.0	7.0	7.0
226.9-keV peak counting statistics	8.2	13.7	16.4
80% HPGe detector efficiency	3.0	3.0	3.0
226.9-keV γ-ray intensity per decay	2.3	2.3	2.3
^{156}Dy natural abundance	5.4	5.4	5.4
Reference foils peak counting statistics (front-back)	3.1–3.1	4.6–5.1	4.1–5.1
40% HPGe detector efficiency	3.0	3.0	3.0
Reference foils γ-ray intensity per decay	0.0015	0.0015	0.0015
Statistical uncertainty of cross section	8.2	13.7	16.4
Systematic uncertainty of cross section	9.5	9.6	9.5
Total uncertainty of cross section	12.6	16.7	19.0
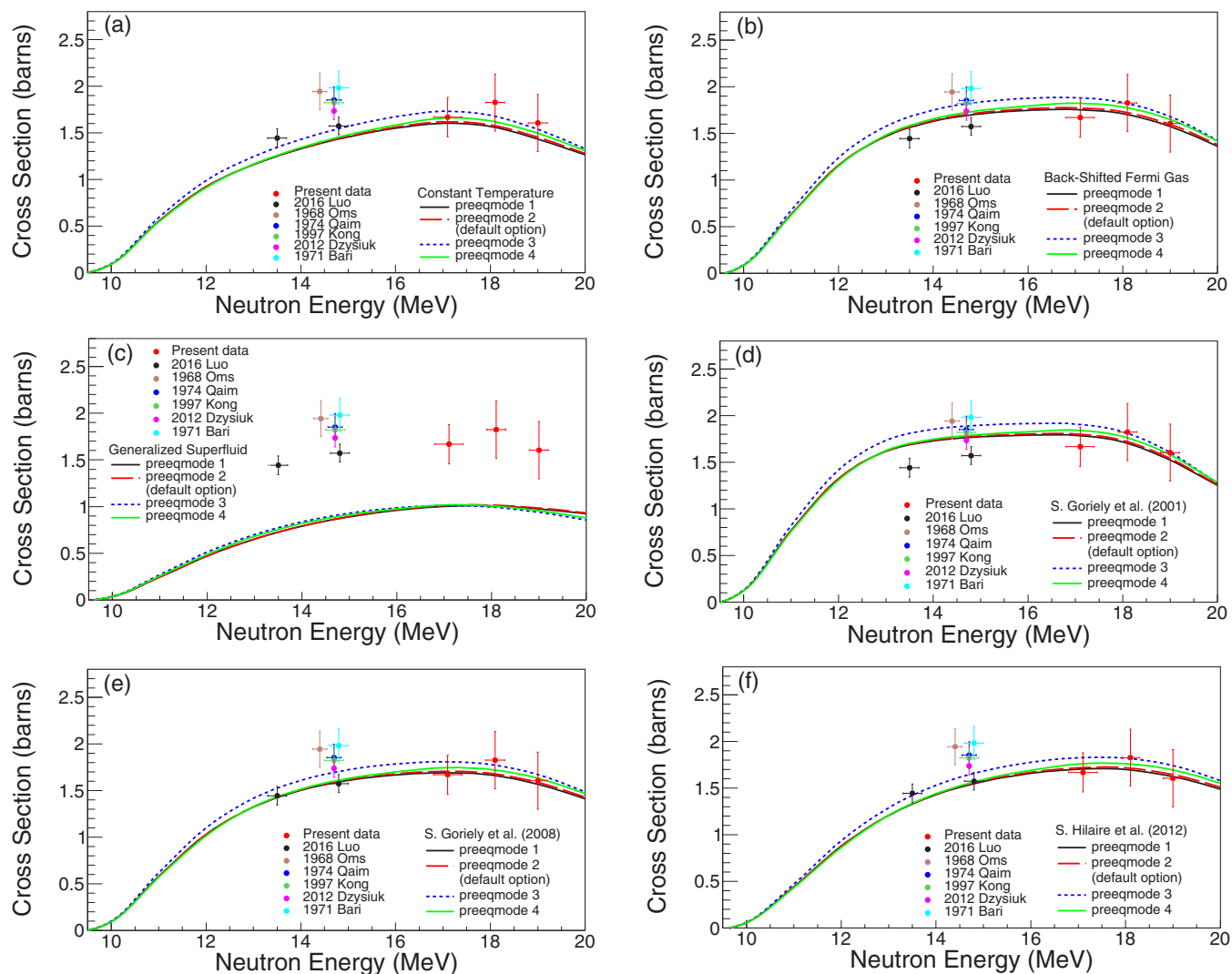
FIG. 3. The TALYS calculations for the ^{156}Dy$(n, 2n)$ ^{155}Dy reaction along with the present and previous measurements [21]. The calculations correspond to each level density model combined with different models for the pre-equilibrium mechanism.

are performed via the Hauser-Feshbach theory [22], whereas the competition between all channels is taken into account.

The TALYS calculations were performed for the default parametrization of the code, as well as by adopting the different models that are incorporated to the code for the level density, the pre-equilibrium mechanism, the γ-ray strength functions, and the optical potential. In this way, the sensitivity of the calculations to the change of these models was tested. Below, the available theoretical models of the code are discussed.

(i) TALYS disposes six different models for the level density. Three of them are phenomenological models: the constant temperature model [23] (keyword: ldmodel 1, default option), the back-shifted Fermi gas model [24] (keyword: ldmodel 2), and the generalized superfluid model [25,26] (keyword: ldmodel 3). The other three models are based on microscopic calculations: Goriely *et al.* (2001) [27] (keyword: ldmodel 4),

Goriely *et al.* (2008) [28] (keyword: ldmodel 5), and Hilaire *et al.* (2012) [29] (keyword: ldmodel 6).

(ii) For the pre-equilibrium mechanism four models are available. Among them the first three perform calculations using the exciton model theory [30–32]: exciton model 1 (keyword: preeqmode 1), exciton model 2 (keyword: preeqmode 2, default option), and exciton model 3 (keyword: preeqmode 3). The last model (keyword: preeqmode 4) is a phenomenological model suggested by Kalbach [33] and it has been developed so as to describe the isotropic part (multistep compound) and the forward peaked part (multistep direct) of the angular distribution of the pre-equilibrium reactions.

(iii) Concerning the γ-ray strength function models, TALYS uses the Brink-Axel Lorentzian one [34,35] for all transitions apart from $E1$. For the $E1$ transition the code offers the option of selecting among eight models: Kopecky-Uhl generlized Lorentzian model [36] (keyword: strength 1, default option), Brink-
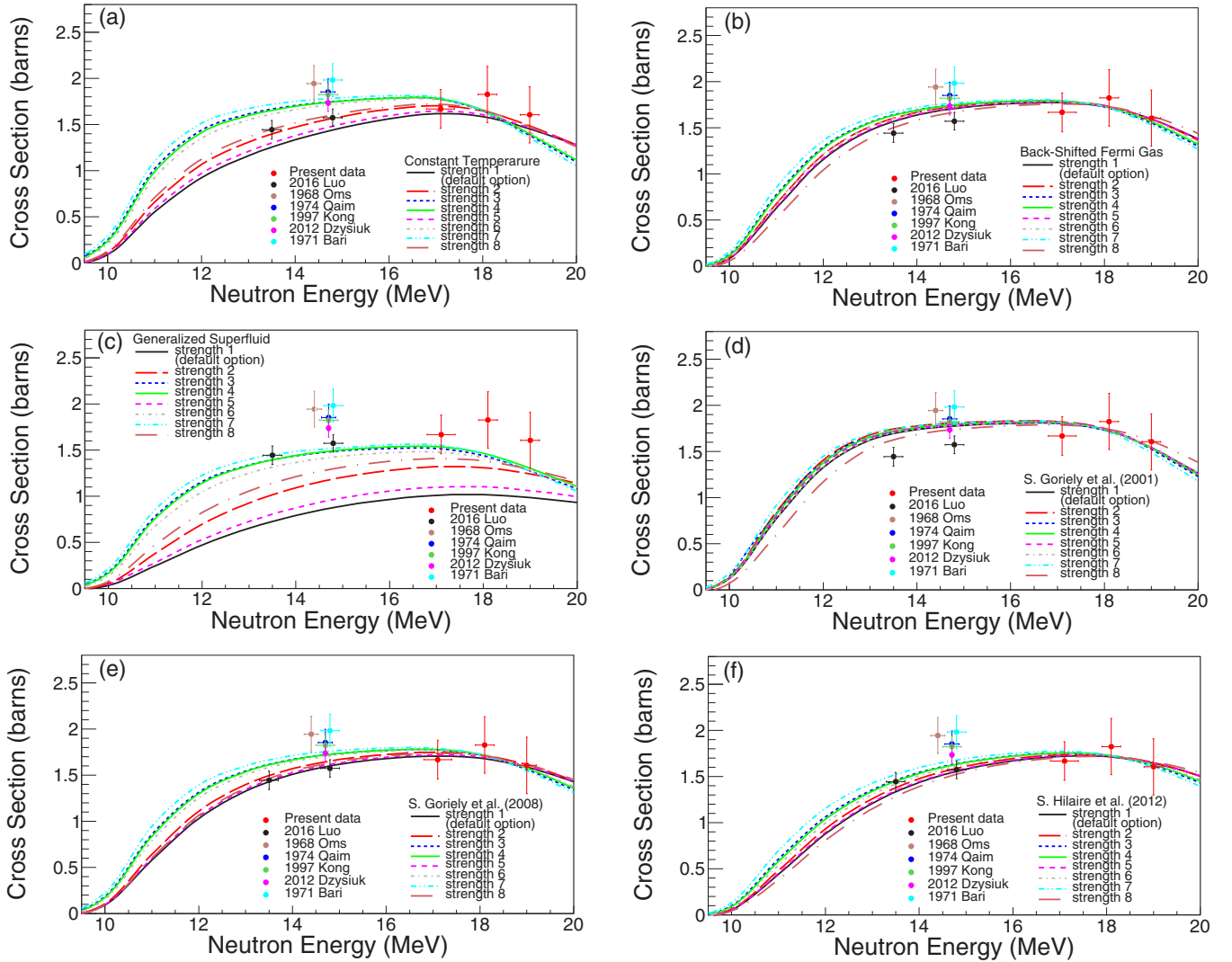
FIG. 4. The TALYS calculations for the ^{156}Dy$(n, 2n)^{155}$Dy reaction along with the present and previous measurements [21]. The calculations correspond to each level density model combined with different models for the γ-ray strength functions of the $E1$ transition.

Axel Lorentzian model [34,35] (keyword: strength 2), Hartree-Fock BCS tables [13] (keyword: strength 3), Hartree-Fock-Bogolyubov (HFB) tables [37] (keyword: strength 4), Goriely's hybrid model [38] (keyword: strength 5), Goriely T-dependent HFB [13] (keyword: strength 6), T-dependent relativistic mean field (RMF) [13] (keyword: strength 7), and Gogny D1M HFB+QRPA [13] (keyword: strength 8).

(iv) The optical model calculations for nucleons are performed via the Koning-Delaroche parametrization [39] (default option), whereas TALYS offers the possibility of replacing this model with the semimicroscopic potential of Bauge *et al.* [40] (keyword: jlmomp y).

In the Hauser-Feshbach calculations the keyword "fullhf y" of TALYS was adopted, which enables the loop over total angular momentum of the ejectile. This keyword is set to "no" by default for time-saving purposes.

Through the calculations it resulted that the larger changes in the excitation function of the reaction under study were observed when different level density models were implemented. Based on this, the calculations were performed at the four stages described below:

(i) adoption of different level density models,
(ii) adoption of different pre-equilibrium models for each level density model,
(iii) adoption of different γ-ray strength function models of the $E1$ transition for each level density model, and
(iv) adoption of different nucleon optical models for each level density model.

In Figs. 3 and 4 the TALYS calculations are presented along with the present and previous measurements. In particular, in Fig. 3 the different models for the pre-equilibrium mechanism have been adopted for each level density model, whereas in Fig. 4 the different models for the γ-ray strength functions of the $E1$ transition have been adopted for each level density model. The calculations of the semimicroscopic

TABLE V. The models and the parametrization of the TALYS code that were used in the calculations of the ^{156}Dy$(n, 2n)$ ^{155}Dy excitation function.

Level density model	Strength function model for the $E1$ transition	Pre-equilibrium mechanism model	Keyword: "fullhf"
Constant temperature (ldmodel 1)	Kopecky-Uhl generalized Lorentzian model (strength 1)	Exciton model 1 (preeqmode 1)	Yes
Back-shifted Fermi gas (ldmodel 2)	Brik-Axel Lorentzian model (strength 2)	Exciton model 2 (preeqmode 2)	
Generalized superfluid (ldmodel 3)	Hartree-Fock BCS tables (strength 3)	Exciton model 3 (preeqmode 3)	
Goriely *et al.* [27] (ldmodel 4)	Hartree-Fock- Bogolyubov tables (strength 4)	Multistep direct/compound model (preeqmode 4)	
Goriely *et al.* [28] (ldmodel 5)	Goriely's hybrid model (strength 5)		
Hilaire *et al.* [29] (ldmodel 6)	Goriely T-dependent HFB (strength 6)		
	T-dependent RMF (strength 7)		
	Gogny D1M HFB + QRPA (strength 8)		

optical potential of Bauge are not presented, as remarkable changes were not revealed in the excitation function of the ^{156}Dy$(n, 2n)$ ^{155}Dy reaction when this model was adopted against the optical model of Koning-Delaroche. In Table V the models and the parametrization of TALYS that were used in the calculations of Figs. 3 and 4 are summarized.

V. RESULTS AND DISCUSSION

Through the present work the cross sections of the ^{156}Dy$(n, 2n)$ ^{155}Dy reaction were measured at neutron beam energies of 17.1, 18.1, and 19.0 MeV. The present data constitute the first of set of measurements at energies higher than 17 MeV and are presented in Table VI.

The present and previous experimental data were compared to theoretical calculations based on TALYS. It resulted that the TALYS calculations have a strong dependence on the selection of the level density model. Concerning the pre-equilibrium models, a general conclusion that can be drawn is that the the exciton model 1 (preeqmode 1), the exciton model 2 (preeqmode 2), and the exciton model 4 (preeqmode 4) produce similar results, whereas the cross-section calculations based on the exciton model 3 (preeqmode 3) differ from the previous calculations for energies higher than 12 MeV. A dependency of the TALYS calculations on the γ-ray strength function models of the $E1$ transition is also observed.

TABLE VI. Measured cross-section values for the ^{156}Dy$(n, 2n)$ ^{155}Dy reaction.

E_n (MeV)	σ (b)
17.1 ± 0.3	1.67 ± 0.21
18.1 ± 0.2	1.82 ± 0.31
19.0 ± 0.2	1.60 ± 0.30

Another interesting remark that results from the calculations is the failure of the generalized superfluid level density model to describe the excitation function of the ^{156}Dy$(n, 2n)$ ^{155}Dy reaction. In particular, a strong underestimation of the cross section was observed over all energies for this level density model and the default options for the rest of the models. The adoption of different models for the pre-equilibrium mechanism did not improve this behavior. An improvement was achieved when the following models of TALYS were adopted for the strength functions of the $E1$ transition: Hartree-Fock BCS tables (strength 3), Hartree-Fock-Bogolyubov tables (strength 4), Goriely T-dependent HFB (strength 6), and T-dependent RMF (strength 7). However, even for these models a poor reproduction of the data was achieved.

VI. SUMMARY AND CONCLUSIONS

In the present study the cross section of the ^{156}Dy$(n, 2n)$ ^{155}Dy reaction was measured for the first time at energies above 17 MeV, namely, at 17.1, 18.1, and 19 MeV. The adopted method was the activation technique relative to the ^{27}Al(n, α) ^{24}Na reference reaction. The quasi-monoenergetic neutron beams were produced in the 5.5-MV tandem accelerator of N.C.S.R. "Demokritos" via the ^{3}H(d, n) ^{4}He reaction.

The experimental data of the present and previous works were compared to theoretical calculations based on the TALYS code (version 1.95). The calculations were performed for all the available level density models of the code, since it was proven in this and previous studies [4,5] that when different level density models are adopted the calculated excitation functions display important changes. Each level density model was combined with different models for the pre-equilibrium mechanism, the γ-ray strength functions of the $E1$ transition, and the optical potential. The results revealed that the

replacement of the optical potential of Koning-Delaroche with the semimicroscopic potential of Bauge does not affect remarkably the excitation function of the reaction under study. On the other hand, the adoption of different models for the pre-equilibrium mechanism affects slightly the calculated cross sections, especially when the exciton model 3 (preeq-mode 3) is adopted against the rest of the models. Finally, the adoption of different γ-ray strength function models for the $E1$ transition seems also to be a component that affects the calculated excitation function. A similar conclusion resulted also from the study of the ^{165}Ho $(n, 2n)$ ^{164}Ho reaction in Ref. [4].

It is also interesting to note the weakness of the generalized superfluid level density model to reproduce the $(n, 2n)$ channel of ^{156}Dy. In general, the generalized superfluid level density model has been proven to describe very satisfactory the $(n, 2n)$ channel of medium- to heavy-mass nuclei, as it was discussed in Refs. [4,41–43], where the TALYS calculations for the $(n, 2n)$ reaction on the ^{165}Ho, ^{197}Au, ^{191}Ir, and ^{193}Ir isotopes are presented. However, when neutron-deficient isotopes are considered the model seems to fail. This behavior was revealed not only in the present work but also in the study of the neutron-deficient isotope ^{162}Er in Ref. [5]. For this reason, in the framework of the present work, theoretical calculations on other neutron-deficient isotopes in this mass region were also performed. From these calculations the same underestimation with respect to the experimental data of the $(n, 2n)$ reaction channel was observed. This underestimation

was found to be more pronounced in the neutron-deficient isotopes: ^{151}Eu and ^{168}Yb. In these physics cases an improvement of the theoretical calculations was achieved when the generalized superfluid level density model was combined with the following models for the γ-ray strength functions of the $E1$ transition: Hartree-Fock BCS tables (strength 3), Hartree-Fock-Bogolyubov tables (strength 4), Goriely T-dependent HFB (strength 6), T-dependent RMF (strength 7), and Gogny D1M HFB+QRPA (strength 8).

[1] E. Dupont, M. Bossant, R. Capote, A. D. Carlson, Y. Danon, M. Fleming, Z. Ge, H. Harada, O. Iwamoto, N. Iwamoto, A. Kimura, A. J. Koning, C. Massimi, A. Negret, G. Noguere, A. Plompen, V. Pronyaev, G. Rimpault, S. Simakov, A. Stankovskiy, W. Sun, A. Trkov, H. Wu, and K. Yokoyama, EPJ Web Conf. **239**, 15005 (2020).

[2] S. Goriely, S. Hilaire, and A. J. Koning, Astron. Astrophys. **487**, 767 (2008).

[3] E. Georgali, N. Patronis, A. Anastasiadis, M. Axiotis, S. Harissopulos, K. Karfopoulos, M. Kokkoris, A. Lagoyannis, C. Potiriadis, and R. Vlastou, Nucl. Instrum. Methods Phys. Res., Sect. A **985**, 164711 (2021).

[4] E. Georgali, N. Patronis, A. Anastasiadis, X. Aslanoglou, M. Axiotis, Z. Eleme, S. Harissopulos, A. Kalamara, K. Karfopoulos, M. Kokkoris, A. Lagoyannis, M. Peoviti, C. Potiriadis, M. I. Savva, I. E. Stamatelatos, M. E. Stamati, A. Stamatopoulos, E. Vagena, T. Vasilopoulou, and R. Vlastou, Phys. Rev. C **102**, 034610 (2020).

[5] E. Georgali, Z. Eleme, N. Patronis, X. Aslanoglou, M. Axiotis, M. Diakaki, V. Foteinou, S. Harissopulos, A. Kalamara, M. Kokkoris, A. Lagoyannis, N. G Nicolis, G. Provatas, A. Stamatopoulos, S. Stoulos, A. Tsinganis, E. Vagena, R. Vlastou, and S. M. Vogiatzi, Phys. Rev. C **98**, 014622 (2018).

[6] J. Luo, L. An, and L. Jiang, J. Radioanal. Nucl. Chem. **308**, 649 (2016).

[7] N. Dzysiuk, A. Kadenko, I. Kadenko, and G. Primenko, Phys. Rev. C **86**, 034609 (2012).

[8] X. Kong, Y. Wang, J. Yang, and J. Yuan, Radiochim. Acta **76**, 11 (1997).

[9] S. M. Qaim, Nucl. Phys. A **224**, 319 (1974).

[10] A. Bari, Diss. Abstr. B **32**, 5091 (1972)

[11] L. A. Oms, J. M. Palms, P. Venugopala Rao, R. E. Wood, and R. W. Fink, Bull. Am. Phys. Soc. **13**, 1699(CA9) (1968).

[12] National Nuclear Data Center, Nuclear Wallet Cards, database version of 7/10/2019, available at https://www.nndc.bnl.gov/wallet/wallet11.pdf.

[13] A. J. Koning, S. Hilaire, and M. C. Duijvestijn, TALYS-1.0, in *Proceedings of the International Conference on Nuclear Data for Science and Technology, April 22–27, 2007, Nice, France*, edited by O. Bersillon, F. Gunsing, E. Bauge, R. Jacqmin, and S. Leray (EDP Sciences, Les Ulis, France, 2008), pp. 211–214.

[14] International Reactor Dosimetry and Fusion File IRDFF, version 1.05, October 9, 2014, https://www-nds.iaea.org/IRDFF/; R. Capote, K. I. Zolotarev, V. G. Pronyaev, and A. Trkov, J. ASTM Int. **9**, 104119 (2012); E. M. Zsolnay, R. Capote, H. K. Nolthenius, and A. Trkov, IAEA Technical Report INDC(NDS)-0616, 2012.

[15] E. Birgersson and G. Lovestam, JRC Science Hub Technical Report, Ref. No. 23794, 2009.

[16] J. F. Ziegler, J. P. Biersack, and M. D. Ziegler, SRIM-2008. Available at http://www.srim.org/SRIM/SRIMLEGL.htm.

[17] S. Agostinelli *et al.*, GEANT4—A simulation toolkit, Nucl. Instrum. Methods. Phys. Res. Sect. A **506**, 250 (2003); IEEE Trans. Nucl. Sci. **53**, 270 (2006); Nucl. Instrum. Methods. Phys. Res. Sect. A **835**, 186 (2016).

[18] N. Nica, Nucl. Data Sheets **160**, 1 (2019).

[19] M. J. Martin, Nucl. Data Sheets **114**, 1497 (2013).

[20] R. B. Firestone, Nucl. Data Sheets **108**, 2319 (2007).

[21] Experimental Nuclear Reaction Data, January 12, 2021, https://www-nds.iaea.org/exfor/exfor.htm.

[22] W. Hauser and H. Feshbach, Phys. Rev. **87**, 366 (1952).

[23] A. Gilbert and A. G. W. Cameron, Can. J. Phys. **43**, 1446 (1965).

[24] W. Dilg, W. Schantl, H. Vonach, and M. Uhl, Nucl. Phys. A **217**, 269 (1973).

[25] A. V. Ignatyuk, K. K. Istekov, and G. N. Smirenkin, Yad. Fiz. **29**, 875 (1979) [Sov. J. Nucl. Phys. **29**, 450 (1979)].

[26] A. V. Ignatyuk, J. L. Weil, S. Raman, and S. Kahane, Phys. Rev. C **47**, 1504 (1993).

[27] S. Goriely, F. Tondeur, and J. M. Pearson, At. Data Nucl. Data Tables **77**, 311 (2001).

[28] S. Goriely, S. Hilaire, and A. J. Koning, Phys. Rev. C **78**, 064307 (2008).

[29] S. Hilaire, M. Girod, S. Goriely, and A. J. Koning, Phys. Rev. C **86**, 064317 (2012).

[30] A. J. Koning and M. C. Duijvestijn, Nucl. Phys. A **744**, 15 (2004).

[31] J. J. Griffin, Phys. Rev. Lett. **17**, 478 (1966).

[32] E. Gadioli and P. E. Hodgson, *Pre-equilibrium Nuclear Reactions* (Oxford University Press, New York, 1992).

[33] C. Kalbach, Phys. Rev. C **37**, 2350 (1988).

[34] D. M. Brink, Nucl. Phys. **4**, 215 (1957).

[35] P. Axel, Phys. Rev. **126**, 671 (1962).

[36] J. Kopecky and M. Uhl, Phys. Rev. C **41**, 1941 (1990).

[37] R. Capote, M. Herman, P. Oblozinsky, P. G. Young, S. Goriely, T. Belgya, A. V. Ignatyuk, A. J. Koning, S. Hilaire, V. Plujko, M. Avrigeanu, O. Bersillon, M. B. Chadwick, T. Fukahori, S. Kailas, J. Kopecky, V. M. Maslov, G. Reffo, M. Sin, E. Soukhovitskii *et al.*, Nucl. Data Sheets **110**, 3107 (2009).

[38] S. Goriely, Phys. Lett. B **436**, 10 (1998).

[39] A. J. Koning and J. P. Delaroche, Nucl. Phys. A **713**, 231 (2003).

[40] E. Bauge, J. P. Delaroche, and M. Girod, Phys. Rev. C **63**, 024607 (2001).

[41] A. Kalamara, R. Vlastou, M. Kokkoris, N. G. Nicolis, N. Patronis, M. Serris, V. Michalopoulou, A. Stamatopoulos, A. Lagoyannis, and S. Harissopulos, Phys. Rev. C **97**, 034615 (2018).

[42] A. Kalamara, R. Vlastou, M. Kokkoris, S. Chasapoglou, A. Stamatopoulos, N. Patronis, M. Serris, A. Lagoyannis, and S. Harissopulos, Phys. Rev. C **98**, 034607 (2018).

[43] A. Kalamara, N. Patronis, R. Vlastou, M. Kokkoris, S. Chasapoglou, A. Stamatopoulos, M. Serris, V. Paneta, M. Axiotis, A. Lagoyannis, S. Harissopulos, and I. E. Stamatelatos, Eur. Phys. J. A **55**, 187 (2019).